Direct formation of nanophase hydroxyapatite on cathodically polarized electrodes

M. SHIRKHANZADEH
Department of Materials and Metallurgical Engineering, Queen's University, Kingston, Ontario, Canada K7L 3N6

Ultrafine-grained, nanophase coatings of hydroxyapatite were synthesized by electrocrystallization from dilute electrolytes ([Ca] = 6.1×10^{-4} M, [phosphate] = 3.6×10^{-4} M) at pH values comparable with the biological pH. At these comparatively low supersaturations, hydroxyapatite is shown to be precipitated without the formation of a precursor phase. A description of the sequence of events occurring at the electrode–electrolyte interface is given to explain the mechanism involved in the direct formation of nanophase hydroxyapatite on polarized electrodes. © *1998 Chapman & Hall*

1. Introduction

Hydroxyapatite (HA) is well established as a bioactive ceramic capable of forming strong chemical bonds with natural bone [1]. The ability to bond chemically to bone is a significant distinction between hydroxyapatite and biocompatible surgical alloys such as Ti6Al4V. A shortcoming of hydroxyapatite ceramic, however, lies in its brittleness and insufficient strength. Despite this, hydroxyapatite ceramic with a well-designed microstructure can be effectively used as a coating on metallic implants. In the field of advanced ceramics, grain-size reduction has been an important method of improving materials' properties. The small grain sizes allow for more efficient deformation mechanism (e.g. diffusion creep) and more effective crack dissipation than is normally available in coarse-grained ceramics [2]. Electrodeposition is potentially an attractive route for applying crystalline phosphate coatings on metallic substrates and has been widely used in the automotive industry [3]. However, the use of this technique for fabricating pure and fine-grained hydroxyapatite coatings suitable for medical applications has been hindered by the poor understanding of the mechanism involved in electrodeposition of calcium phosphate phases from aqueous solutions. In an earlier work, we reported that nanophase apatite coatings can be synthesized on cathodically polarized electrodes, using electrolytes containing dissolved calcium and phosphate ions at pH 4.4 [4]. However, these coatings were found to be octacalcium phosphate (OCP)-type apatite and contained acid phosphate groups. Steam treatment followed by calcining at 425 °C [4] or a post-treatment in alkaline solutions [5] was necessary to convert these coatings into pure hydroxyapatite coatings. Subsequent to this work, Redpenning *et al.* [6] also demonstrated that brushite ($CaHPO_4 . 2H_2O$) coatings may be converted to hydroxyapatite by treatment in alkaline solutions. However, hydroxyapatite coating prepared by this route, similar to the brushite precursor phase, consisted of sharp and fragile crystals as large as 30–50 μm and exhibited undesirable microstructures and morphologies. Moreover, because of the large sizes of the precursor crystals, complete transformation of brushite to hydroxyapatite may not be achieved and thus the coating obtained by this route may contain impurities such as amorphous calcium phosphate (ACP).

In view of the significance of synthesizing pure and fine-grained hydroxyapatite coatings suitable for medical applications, further studies are required to elucidate the mechanism involved in the precipitation of hydroxyapatite on cathodically polarized electrodes. In the present work, evidence is provided to show that at very low concentrations of calcium and phosphate ions and at pH values comparable with the biological pH, nanophase hydroxyapatite can indeed be deposited on the cathodically polarized electrodes without the formation of a precursor phase. A description of the sequence of events occurring at the electrode–electrolyte interface during the electrodeposition process is given to explain the mechanism involved in formation of nanophase hydroxyapatite under these conditions.

2. Experimental procedure

The electrolytes used for the electrodeposition of calcium phosphate coatings were prepared by dissolving reagent-grade $Ca(NO_3)_2$ and $NH_4H_2PO_4$ in deionized water. To show the significance of the concentrations and the pH of the electrolyte in the formation of nanophase hydroxyapatite, electrolytes with varying concentrations of calcium and phosphate ions were employed. $NaNO_3$ ($[NO_3^-] = 0.1$ M) was also added to improve the ionic strength of the electrolytes. The pH of the electrolytes was adjusted so that in all cases electrolytes were saturated with respect to hydroxyapatite. Table I shows the adjusted pH

TABLE I Concentrations and the pH of the electrolytes saturated with respect to hydroxyapatite

Total calcium T_{Ca} (mM)	Total phosphate T_p (mM)	pH (adjusted)
20	12.0	4.2
10	6.0	4.5
5.0	3.0	4.7
2.5	1.5	5.3
1.25	0.75	5.6
0.61	0.36	6.0

values for saturated solutions containing various concentrations of calcium and phosphate ions. These pH values were determined from the solubility isotherm for hydroxyapatite in the ternary system $Ca(OH)_2$–H_3PO_4–H_2O [7]. Electrodeposition of calcium phosphates was carried out for 2 h at 85 °C in a conventional cell fitted with a saturated calomel electrode (SCE). Commercially pure titanium plates pre-etched in hydrofluoric acid were used as the substrate (cathode) for deposition of calcium phosphates. CO_2-free nitrogen was continuously sparged into the electrolyte during the electrodeposition process to minimize the risk of contamination of the deposits with carbonates. A Hokuto Denko (HD) HAB-151 potentionstat/galvanostat operating in potentiostatic mode was employed to maintain the cathode potential at -1400 mV (versus SCE). The microstructure of the calcium phosphate deposits was determined by the glancing angle X-ray diffraction (XRD) technique using Cr K_α ($\lambda = 0.229\,092$ nm) radiation. Scanning electron microscopy (SEM) and transmission electron microscopy (TEM) were also used to examine the morphology and crystal habits of the calcium phosphate deposits. Samples for TEM analysis were prepared by placing fine powder of calcium phosphates scraped from the substrate on carbon-coated copper grids. Fourier transform–infrared (FT–IR) spectroscopy was also used to determine the chemical composition of the deposits.

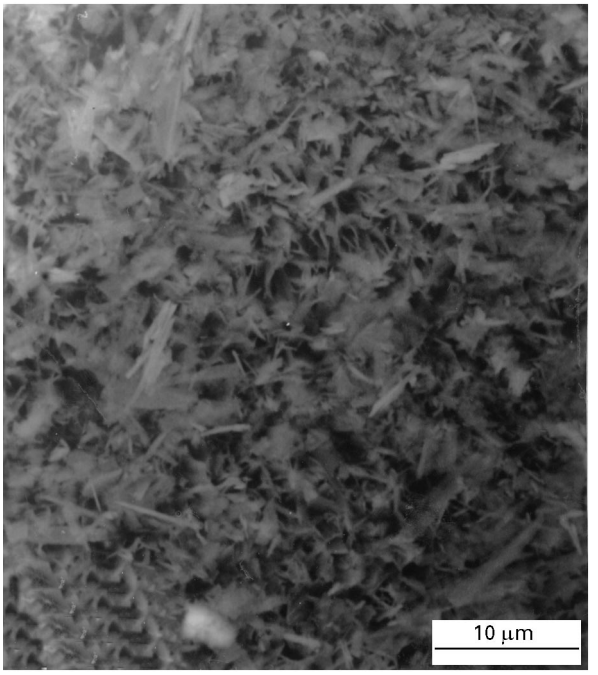

Figure 1 Scanning electron micrograph of the calcium phosphate coating obtained from the acidic electrolyte at pH = 4.2.

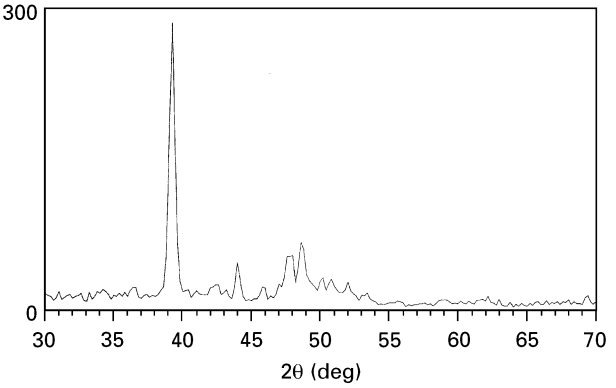

Figure 2 Thin-film X-ray diffraction of the calcium phosphate coating obtained from the acidic electrolyte at pH = 4.2.

3. Results and discussion

3.1. Morphology and crystal structure of calcium phosphate deposits

Marked changes in the morphology and crystal structure of calcium phosphate deposits were observed as the pH of the electrolyte increased from 4.2 to 6.0. At acidic pH values (ca. pH ~ 4.2) the deposits consisted of a network of relatively large plate-like crystals in the range of 4–6 μm (Fig. 1). The X-ray diffraction pattern of these deposits is shown in Fig. 2. It is seen that the deposits formed under these conditions exhibit apatitic characteristics similar to bone apatite and non-stoichiometric hydroxyapatite [8]. The X-ray peaks at $2\theta = 39°$ and 47°–52° in the diffraction pattern can be attributed to the (0 0 2) plane and to a combination of the poorly resolved 2 1 1, 1 1 2 and 3 0 0 planes of hydroxyapatite. Thus, although apatite-like in their general structural features, deposits formed from saturated electrolytes at acidic pH values deviate markedly from stoichiometric hydroxyapatite in structural details. Moreover, the poorly resolved reflections of the X-ray pattern of these deposits makes it impossible to exclude on OCP-like structural interpretation. The octacalcium phosphate (OCP) precursor model proposed by Brown [9] to explain the formation of non-stoichiometric apatites may, in fact, provide a possible interpretation of the sequence of events that take place during the electrodeposition of calcium phosphates from acidic electrolytes. In Brown's proposal, the first crystals formed as a precursor to apatite are postulated to be two-dimensional growth of single unit-cell thick OCP. This growth pattern would account for the flaky appearance of the crystals observed in the present work.

As the pH of the electrolyte increased, the size of the crystals formed on the cathode decreased and the X-ray diffraction of the deposits became more

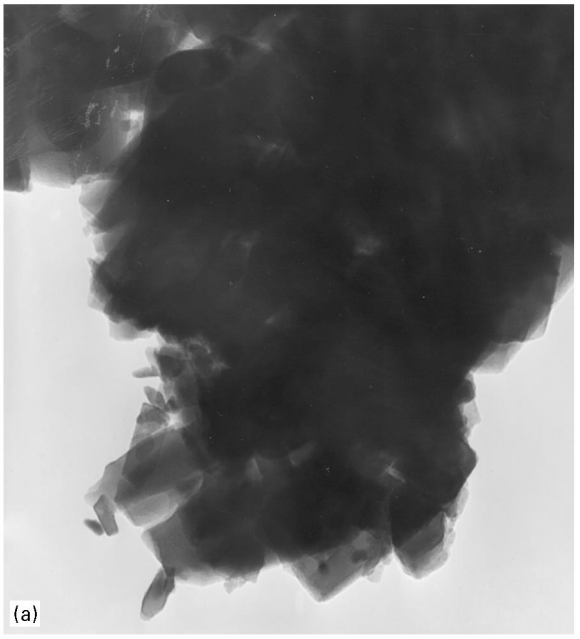

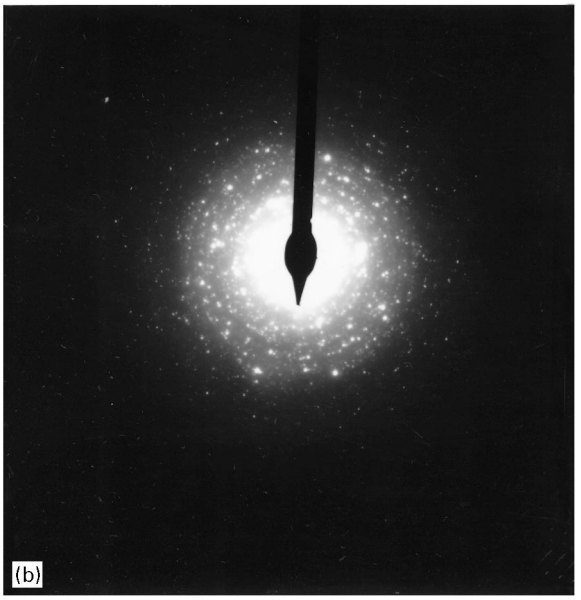

Figure 3 (a) Transmission electron micrograph showing the fine-grained structure of the hydroxyapatite deposit obtained at pH = 6.0, and (b) the "ring-spot" electron diffraction pattern of the same specimen.

resolved. At the highest pH value employed (pH = 6.0), the deposit consisted of very fine crystals in the nanometre range (Fig. 3a and b) and the X-ray diffraction pattern (Fig. 4) indicated major peaks corresponding to 002, 102, 210, 211, 300 and 202 reflections of hydroxyapatite. The results thus indicate that under these conditions, hydroxyapatite may form directly on the cathode surface. As shown in Table I, the concentration of calcium and phosphate ions at pH 6.0 is very low. Thus, the level of supersaturation may be in the range which exists *in vivo* at the sites of calcification. This may explain the low rate of crystal growth and formation of nanometre-sized crystals under these conditions.

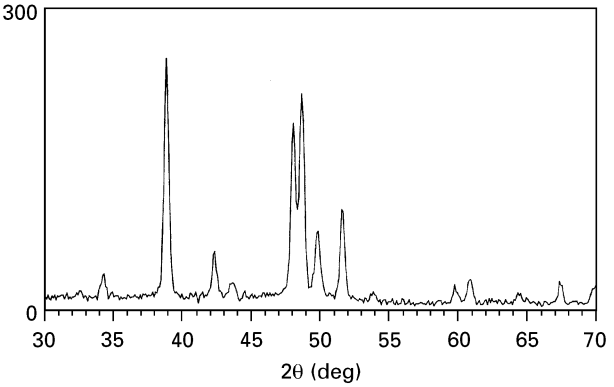

Figure 4 Thin-film X-ray diffraction of the hydroxyapatite coating obtained from the electrolyte at pH = 6.0.

3.2. FT–IR analysis of calcium phosphate deposits

The strong influence of the electrolyte pH on the crystal structure of calcium phosphate deposits was also confirmed by the FT-IR analysis. The ν_1 and ν_3 phosphate bands in the 900–1200 cm^{-1} and the ν_4 absorption bands in the 500–700 cm^{-1} spectral region were used to characterize the structure of the apatite formed at various pH values (Fig. 5). The spectral range 900–1200 cm^{-1} contains the symmetric (ν_1) and the asymmetric (ν_3) P–O stretching modes of the phosphate groups. It is known that for hydroxyapatite, the symmetric P–O stretching mode occurs at 962 cm^{-1} while the asymmetric (ν_3) stretching modes occur at 1050 and 1100 cm^{-1} [11]. As seen in Fig. 5, the infrared bands at 961, 1050 and 1100 cm^{-1}, corresponding to hydroxyapatite, become more resolved and intense as the pH of the electrolyte is increased. It is also seen that at low pH values, a peak at 925 cm^{-1} appears which is assigned to acid phosphate groups (HPO_4^{2-}). The intensity of this peak gradually diminishes as the pH increases, signifying elimination of the acid phosphate contaminates. Similar changes were also observed in the 500–700 cm^{-1} spectral region. The bands in the 570 and 605 cm^{-1} regions can be assigned as members of the antisymmetric bending motion of phosphate groups in hydroxyapatite [11], while the band at 632 cm^{-1} is assigned to a vibrational mode of the OH ions in hydroxyapatite [12]. The results in Fig. 5 clearly indicate that the deposits formed at relatively low pH values are deficient in hydroxyl ions. The hydroxyl deficiency in the deposits formed at low pH was further confirmed by the lack of substantial OH stretching band at $\sim 3600\ cm^{-1}$ (Fig. 6). These deposits also exhibited HPO_4^{2-} absorption peak at 525 cm^{-1} very close to that observed for crystalline acid phosphates, signifying the presence of OCP–apatite interlayering similar to bone apatite [13]. As the pH of the saturated electrolytes increased, the acid phosphate peak at 525 cm^{-1} decreased and the OH peaks at ~ 632 and 3600 cm^{-1} increased. At the highest pH value employed (pH = 6.0), the deposits formed on the cathode exhibited only absorption bands associated with hydroxyapatite. Thus the FT–IR results further confirmed that under these conditions hydroxyapatite may be deposited directly without the formation of a precursor phase.

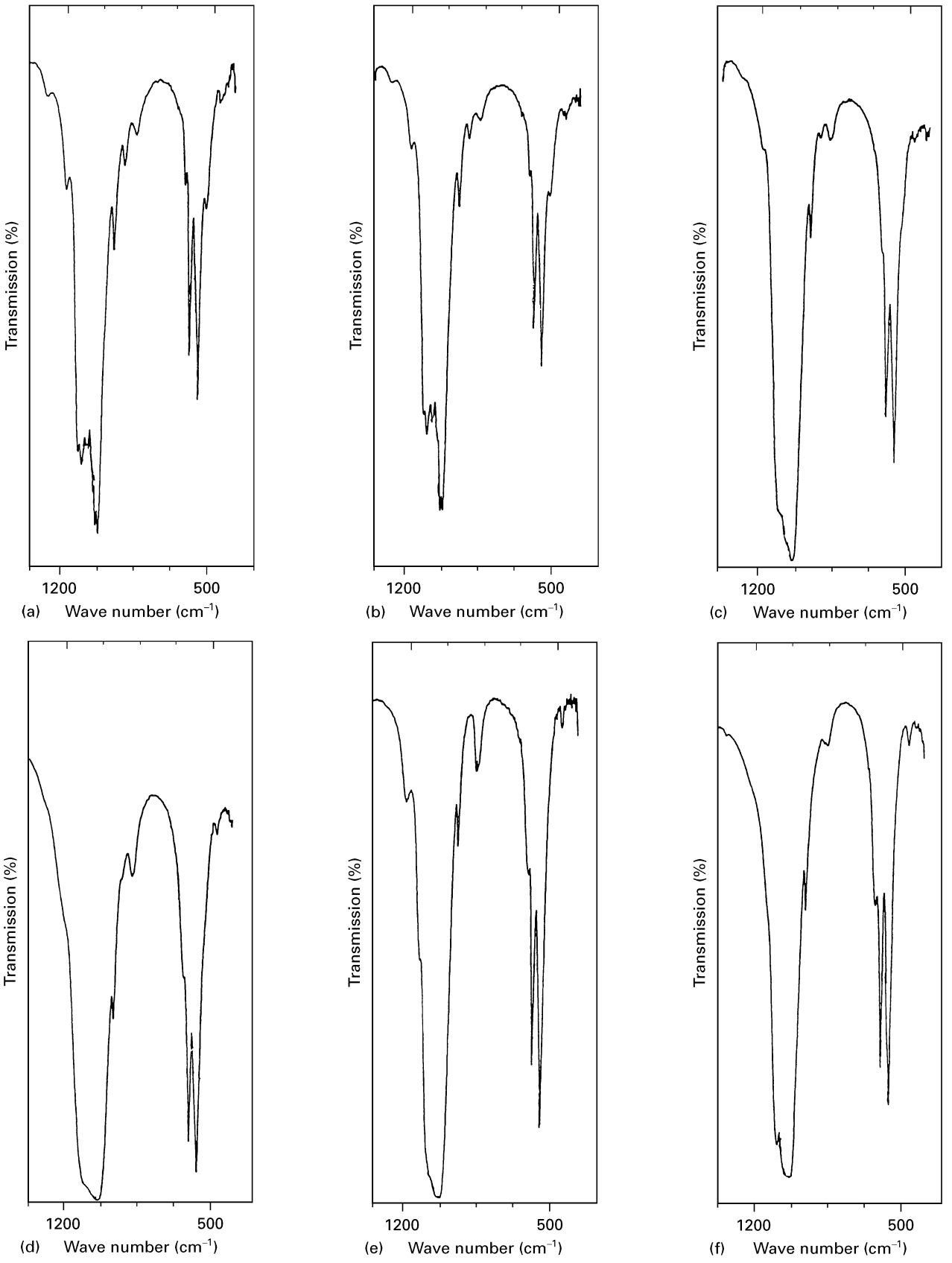

Figure 5 FT–IR spectra of the calcium phosphate deposits obtained from saturated electrolytes at various pH values: (a) pH = 4.2, (b) pH = 4.5, (c) pH = 4.7, (d) pH = 5.3, (e) pH = 5.6, and (f) pH = 6.0.

3.3. Mechanism of direct formation of hydroxyapatite on cathodically polarized electrodes

Precipitation of calcium phosphates on cathodically polarized electrodes occurs through a nucleation and growth mechanism. Fig. 7 shows a simplified schematic diagram of the cathode–electrolyte interface and the active ionic species participating in the interfacial reactions during the electrodeposition of calcium phosphates. In general, the formation of the calcium

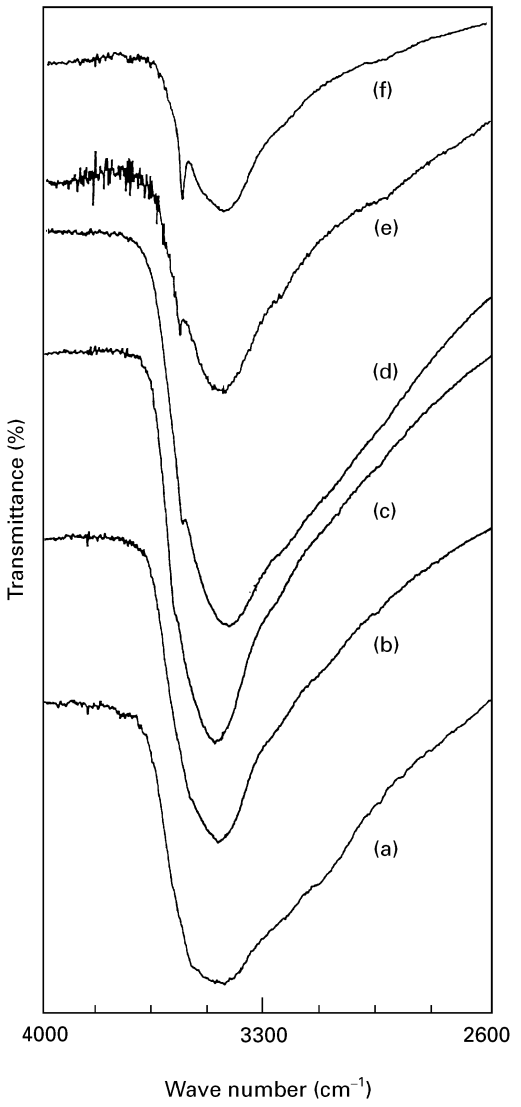

Figure 6 FT–IR spectra of the calcium phosphate deposits in the range 2600–4000 cm^{-1} indicating hydroxyl deficiency at low pH values: (a) pH = 4.2, (b) pH = 4.5, (c) pH = 4.7, (d) pH = 5.3, (e) pH = 5.6, and (f) pH = 6.0.

phosphates on the cathode is initiated once the level of supersaturation exceeds the critical level required for the nucleation of these compounds. During the electrodeposition process, the pH of the electrolyte in the close vicinity of the cathode is increased as a result of the electrolysis. This causes the supersaturation level to raise and thus various calcium phosphates may precipitate on the cathode surface. In the case of acidic electrolytes (pH $\sim$ 4.2), the activity of hydrogen ions is relatively high and thus the local pH is mainly increased as a result of the electro-reduction of hydrogen ions

$$2H^+ + 2e^- \rightarrow H_2 \quad (1)$$

The rapid consumption of H^+ ions at the cathode surface leads to a significant increase in the local pH within the diffusion layer. Hydrogen ions continuously reach the cathode surface from the bulk of the electrolyte by diffusion. The driving force for the diffusion process is the concentration difference, $\Delta C = C_{H^+,b} - C_{H^+,s}$, where $C_{H^+,b}$ and $C_{H^+,s}$ are the bulk concentration and the surface concentration of

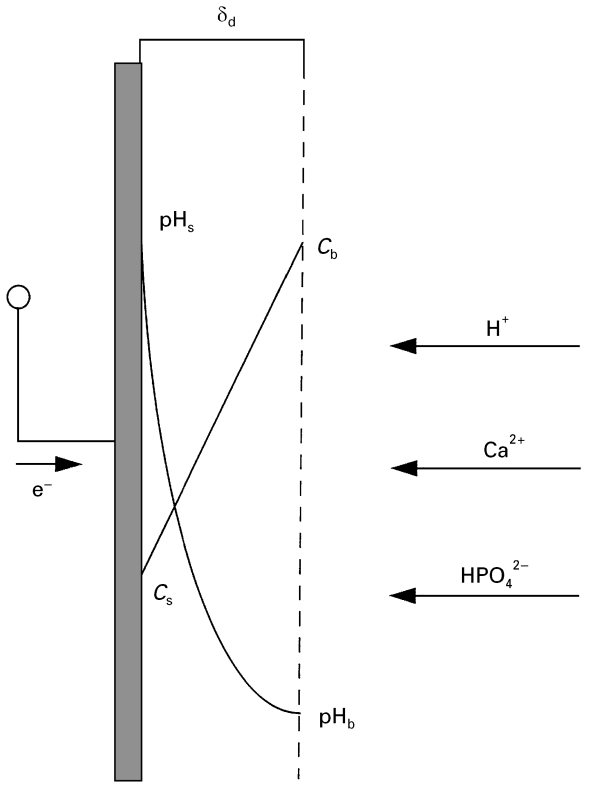

Figure 7 Simplified schematic diagram of the cathode–electrolyte interface showing the variation of H^+ ion concentration and the pH within the diffusion layer.

H^+ ions at the cathode surface, respectively. Assuming a linear concentration profile within the diffusion layer, the local concentration of H^+ ions may be given by

$$C_{H^+,x} = (C_{H^+,b} - C_{H^+,s})\frac{x}{\delta_d} + C_{H^+,s} \quad (2)$$

where δ_d is the thickness of the diffusion layer and x is the distance from the cathode surface. At relatively high overpotentials normally encountered in electrodeposition of calcium phosphates, H^+ ions are expected to be consumed rapidly, and thus the concentration of H^+ ions at the cathode surface would be extremely small compared with the bulk concentration. Therefore, the pH of the electrolyte within the diffusion layer may be given by

$$pH = pH_b - \log\frac{x}{\delta_d} \quad (3)$$

where pH_b is the pH of the bulk electrolyte. Equation 3 shows that for $x > 0$ the local pH may be strongly influenced by the pH of the electrolyte. The local pH within the diffusion layer is an important parameter which directly affects the local concentration of acid phosphate groups in accordance with the following equilibrium [14]

$$H^+ + PO_4^{3-} \rightleftharpoons HPO_4^{2-} \quad (4a)$$

$$K_{eq} = 2.33 \times 10^{12} \quad (4b)$$

Thus, depending on the pH of the bulk electrolyte, calcium phosphate crystals grown on the cathode may contain various amounts of acid phosphate groups.

The FT–IR results in the Fig. 5 indeed show that calcium phosphates deposited from the saturated solutions at acidic pH values contain a substantial amount of acid phosphate groups. The results thus indicate that under these conditions, a sufficiently alkaline pH may not be attained in the close vicinity of the cathode for the complete transformation of acid phosphate groups. Previous work [4] has shown that the acid phosphate content of the deposits cannot be appreciably reduced by increasing the cathode potential to -1600 mV (versus SCE). Thus although H^+ ions can be consumed relatively fast at -1600 mV, the intense hydrogen gas evolution at this potential seems to enhance the mass transfer of H^+ ions and prevent the local pH increasing significantly in the vicinity of the cathode. Attempts to eliminate acid phosphate by employing potentials higher than -1600 mV were also unsuccessful. The intense hydrogen evolution at these potentials practically prevented calcium phosphate from precipitating on the cathode. In contrast, the pH of the electrolyte proved to be an effective parameter for controlling the acid phosphate content of the deposits. As the pH of the electrolyte increased, the acid content of the deposits sharply decreased. At the highest pH value employed (pH = 6.0), the acid phosphate groups were effectively eliminated and the calcium phosphate deposits consisted of nanometre-sized hydroxyapatite crystals. It is important to note that at such relatively high pH values, the activity of hydrogen ions is very low and thus the electro-reduction of water molecules and other oxidizing agents present in the electrolyte may play a predominant role in the pH increase at the cathode surface. Reduction of water molecules under these conditions may result in the formation of numerous hydroxyl groups on the cathode surface

$$2H_2O + 2e^- \rightarrow H_2 + 2(OH)^-_{ads} \quad (5)$$

The hydroxyl ions generated at the cathode surface may effectively react with the acid phosphates to form surface PO_4^{3-} species. Transformation of the acid phosphates to PO_4^{3-} species on the cathode surface may be represented by

$$HPO_4^{2-} + (OH)^-_{ads} \rightarrow H_2O + PO_4^{3-} \quad (6)$$

Thus under these conditions, the solution in the close vicinity of the cathode may become effectively undersaturated with respect to OCP. In addition, at pH $\sim$ 6, the electro-reduction of the oxide film present on the cathode may also result in the formation of the physisorbed hydroxyls and chemisorbed OH (i.e. Ti–OH)

$$TiO_2 + 2H_2O + e^- \rightarrow Ti(OH)_3 + (OH)^-_{ads} \quad (7)$$

The adsorbed hydroxyl groups may play an essential role in the nucleation of hydroxyapatite on the cathode surface. The significance of hydroxyl groups in the nucleation of apatite on bioglass and sol–gel silica and titania has indeed been emphasized by a number of researchers [15, 16]. Thus, although the level of supersaturation at pH 6.0 may be too low for precipitation of OCP as a precursor phase, the presence of the adsorbed hydroxyl groups on the cathode surface may provide numerous sites for direct nucleation of hydroxyapatite from these dilute solutions in accordance with the following reaction

$$10\,Ca^{2+} + 6\,PO_4^{3-} + 2\,(OH)^-_{ads} \rightarrow Ca_{10}(PO_4)_6(OH)_2 \quad (8)$$

4. Conclusion

The results in this work have shown that the nature of calcium phosphate phases deposited on the cathodically polarized electrodes from electrolytes saturated with respect to hydroxyapatite, strongly depends on the pH of the electrolyte. Deposits precipitated from acidic electrolytes consisted of plate-like crystals in the range of 4–6 μm and deviated markedly from stoichiometric hydroxyapatite. The formation of these deposits may be explained by an OCP precursor model. On the other hand, the results in this work show that at very low concentrations of calcium and phosphate ions and at pH values comparable with the biological pH, nanophase hydroxyapatite can be directly deposited on the cathodes without the formation of a precursor phase.

Acknowledgements

The author thanks the Natural Sciences and Engineering Research Council of Canada (NSERC) for the financial support provided for this research project, and Dr I. Rauf for his assistance regarding TEM analysis.

References

1. M. JARCHO, *Clin. Orthop. Rel. Res.* **157** (1981) 259.
2. R. W. SIEGEL, S. RAMASAMY, H. HAHN, LI ZONGQUAN, LU TING and R. GRONSKY, *J. Mater. Res.* **3** (1988) 1367.
3. G. LORIN, "Phosphating of Metals" (Finishing Publication Limited, London, 1974).
4. M. SHIRKHANZADEH, *Nanostruct. Mater.* **4** (1994) 677.
5. M. SHIRKHANZADEH and M. AZADEGAN, *Mater. Lett.* **15** (1993) 392.
6. J. REDPENNING, T. SCHLESSINGER, S. BURNHAM, L. LIPPIELO and J. MIYANO, *J. Biomed. Mater. Res.* **30** (1996) 287.
7. W. E. BROWN, US Pat. 4518 430 (1985).
8. M. SHIRKHANZADEH, *Mater. Sci. Lett.* **10** (1991) 1415.
9. W. E. BROWN, *Clin. Orthop.* **44** (1966) 205.
10. R. E. WUTHIER, G. S. RICE, J. E. B. WALLACE, R. L. WEAVER, R. Z. LE GEROS and E. D. EANES, *Calcif. Tissue Int.* **37** (1985) 401.
11. J. M. STUTMAN, J. D. TERMINE and A. S. POSNER, *Trans. N.Y. Acad. of Sci.* **29** (1966) 669.
12. L. WINAND, PhD thesis, University of Liege, Liege, Belgium, (1960).
13. B. O. FOWLER, E. C. MORENO and W. E. BROWN, *Arch. Oral. Biol.* **11** (1966) 477.
14. G. H. NANCOLLAS, *Corrosion* **39** (1983) 77.
15. M. M. PEREIRA, A. E. CLARK, L. L. HENCH, *J. Amer. Ceram. Soc.* **78** (1995) 2463.
16. P. LI, C. OHTSUKI, T. KOKUBO, K. NAKANISHI, N. SOGA, T. NAKAMURA and T. YAMAMURO, *J. Mater. Sci. Mater. Med.* **4** (1993) 123.

Received 8 January
and accepted 22 May 1997